TU Delft

Delft University of Technology

Document Version
Final published version

Licence
CC BY

Citation (APA)
Singh, S. K., & Groves, R. M. (2026). Study of inner surface behavior and structural integrity of composite liquid hydrogen (LH2) outer tank using a robotic crawler. *Measurement Science and Technology*, *37*(20). https://doi.org/10.1088/1361-6501/ae6937

Important note
To cite this publication, please use the final published version (if applicable).
Please check the document version above.

Copyright
In case the licence states “Dutch Copyright Act (Article 25fa)”, this publication was made available Green Open Access via the TU Delft Institutional Repository pursuant to Dutch Copyright Act (Article 25fa, the Taverne amendment). This provision does not affect copyright ownership.
Unless copyright is transferred by contract or statute, it remains with the copyright holder.

Sharing and reuse
Other than for strictly personal use, it is not permitted to download, forward or distribute the text or part of it, without the consent of the author(s) and/or copyright holder(s), unless the work is under an open content license such as Creative Commons.

Takedown policy
Please contact us and provide details if you believe this document breaches copyrights.
We will remove access to the work immediately and investigate your claim.

This work is downloaded from Delft University of Technology.

Measurement Science
and Technology

PURPOSE-LED
PUBLISHING™

PAPER • OPEN ACCESS

Study of inner surface behavior and structural integrity of composite liquid hydrogen (LH2) outer tank using a robotic crawler

To cite this article: Shishir Kumar Singh and Roger M Groves 2026 *Meas. Sci. Technol.* **37** 205901

View the article online for updates and enhancements.

You may also like

- Robot deployed Laser-Ultrasonic NDT system for inspection of large aircraft structures
Vicki James, Dave Carswell, J Riise et al.
- A study on 3D scan-based robot arm control approach for pulse-echo laser ultrasonic testing of curved composite structures
King Sum Ma, Kyu-Jin Lee and Jung-Ryul Lee
- Structural design and kinematic analysis study of ultrasonic flaw detection robot
Haoran Zhai and Ziming Zhang

This content was downloaded from IP address 154.59.124.113 on 02/06/2026 at 09:02

Measurement Science and Technology

Check for updates

OPEN ACCESS

RECEIVED
31 December 2025

REVISED
10 April 2026

ACCEPTED FOR PUBLICATION
6 May 2026

PUBLISHED
18 May 2026

Original content from this work may be used under the terms of the Creative Commons Attribution 4.0 licence.

Any further distribution of this work must maintain attribution to the author(s) and the title of the work, journal citation and DOI.

PAPER

Study of inner surface behavior and structural integrity of composite liquid hydrogen (LH2) outer tank using a robotic crawler

Shishir Kumar Singh* and **Roger M Groves**

Department of Aerospace Structures and Materials, Delft University of Technology, Kluyverweg 1, Delft 2629, HS, The Netherlands
* Author to whom any correspondence should be addressed.

E-mail: s.k.singh@tudelft.nl

Keywords: automation, phased array, robotic inspection, damage detection

Abstract

Inspection of composite liquid hydrogen tanks (LH2) for aviation is highly challenging using current non-destructive testing techniques. Also, manufacturing of these composite LH2 tanks is challenging due to thermal stresses, making post-manufacturing and in-service inspection essential for safe operations. The external insulating layer and restricted access to the tank's interior are the reasons for this. To inspect the inner curved surfaces of a carbon fiber-reinforced polymer (CFRP) composite tank, a compact, high-payload-ratio ultrasonic probe-based inspection using an autonomous robotic crawler was developed. The developed device offers a workable solution for challenging LH2 tank inspection situations, as it is designed to function through tank apertures as small as 250–300 mm in diameter. For accurate localization on the uneven inner surfaces of the composite LH2 tank, the robot utilizes wheel encoders and features wheeled locomotion. A phase array-based wheel probe for ultrasonic examination, operating at 5 MHz, is used in conjunction with a spring load to ensure proper coupling with the surface. To perform straight-line motion on a CFRP composite surface under dynamic conditions at various speeds, this work examines proportional-integral-derivative tuning for a crawler, combined with an ultrasonic phased array probe, and determines an optimized speed for composite LH2 inspection. The device demonstrates the detection of possible ply drop-off and surface irregularity damage. The findings are important, as an investigation has been conducted to assess the quality of ultrasonic scans on the curved surface with varying thicknesses of the composite tank.

1. Introduction

Hydrogen is a possible alternative fuel for aircraft because of its high specific energy and zero emissions properties. Combustion of liquid hydrogen (LH2) produces no carbon dioxide emissions, only water vapor and minor nitrogen oxides. As a viable substitute for conventional fossil fuels, hydrogen holds great promise for a more sustainable future [1]. Although hydrogen has a high gravimetric energy density, its low volumetric density makes storage and transport significantly more complex than conventional fossil fuels [2]. The development of economical, effective storage techniques that take into account the difficult physicochemical characteristics of hydrogen is essential to its sustainable usage as a future energy carrier [3].

Advances in composite materials have enabled the construction of larger and more intricate liquid hydrogen (LH2) tanks, leading to the development of Type IV vessels, in which carbon fiber bears the structural load, typically with a polymer liner, though at high cost [4]. More recently, Type V liner less fully composite vessels have emerged, but they remain in the pre-commercial stage. For cryogenic applications, maintaining hydrogen in its liquid state at extremely low temperatures (<-253 °C) presents an additional challenge [5]. These challenges can be overcome by the appropriate material selection and design of the tank. Yet, commercialization of LH2 tanks still faces critical obstacles due to leakage

© 2026 The Author(s). Published by IOP Publishing Ltd

through the inner wall of the tank, existing material delamination or debond, and increased permeability due to microcracking of the wall material. Damage due to the combination of thermal cycles, pressure cycles, and external loads (vibration, inertia, etc), and ply drop-offs, all of which can cause failure to the tank integrity and compromise safety [6, 7]. Ultrasonic testing is a key non-destructive testing (NDT) for aerospace composites, capable of detecting delamination, voids, and fiber–matrix debonding with high sensitivity and efficiency. Its adaptability to advanced methods such as phased array and guided waves makes it suitable for ensuring reliability in aerospace, automotive, and structural composite applications [8]. In aerospace-grade carbon fiber reinforced polymer (CFRPs), ultrasonic phased array C-scan is particularly valuable, offering high sensitivity and resolution for characterizing porosity size and distribution across the composite bulk [9]. Phased array ultrasonic testing (PAUT) has the capacity to focus and direct ultrasonic waves at specific angles and has the ability to activate each individual ultrasonic element in a predetermined sequence [10–12]. A phased array can also drive multiple elements and receive and digitize the echoes that are returned in accordance with a delay law. Conventional PAUT is limited by operator-dependent variability, where even slight probe misorientation can introduce significant measurement errors [12]. This limitation highlights the need for robotic PAUT, which ensures consistent probe alignment while enabling simultaneous defect detection and preload measurement with improved accuracy and reliability [13]. Advances in robotics and computer science have sparked significant interest in applying these technologies to the structural health monitoring (SHM) of inaccessible areas of composite tanks. Automation in ultrasonic inspection enables rapid, accurate scans, enhancing efficiency and improving data consistency for the analysis of complex geometry. Robotic devices holding the probe that attach to LH2 storage tanks and move along their surfaces while scanning and inspecting can significantly accelerate the inspection process and reduce human error. Recently, crawling devices have emerged as a viable solution for mobile, unconstrained scanning [14]. This includes multimodal rigid robots—such as mobile robots, flying and perching drones equipped with SHM capabilities using pulse-echo (PE) and ultrasonic surface waves techniques employing one or two robots [15–17]. For instance, researchers have developed climbing robots utilizing permanent magnetic adhesion to perform ultrasonic C-scan inspections of vertical metal infrastructures such as oil tanks [18]. These robotic systems, equipped with wheeled locomotion and encoder-based localization, enable precise data acquisition and reconstruction of C-scan images [18]. The climbing robotic platform has a low load-carrying capacity, more complex control algorithms, limiting the number of non-destructive evaluation (NDE) sensors that can be incorporated for flaw inspection [16]. While PE laser ultrasonic testing offers powerful contactless inspection capabilities for CFRPs for the thin structures, its reliance on bulky and costly systems limits its portability and industrial adoption [19].

Despite progress, many robotic systems are still bulky, expensive, and poorly adaptable, emphasizing the need for compact, affordable, and portable inspection options for large, complex composites. As additive manufacturing technology advances, robotics are built for high payload applications and optimized for specific needs. These materials are widely used for their superior mechanics, cost savings, and suitability for specialized tasks [20, 21].

The robotic inspection system is designed based on key design constraints, including: large-radius but locally uneven composite LH2 tank geometry, conformal surface requirements, accessibility limitations, payload and packaging restrictions, acoustic coupling stability, and the necessity for controlled linear scanning velocity. The primary goal is to inspect an inaccessible tank structure with a system that maintains a high payload ratio while accommodating the curvature and complexity of conformal liquid hydrogen tank (LH2) surfaces. To achieve this, a 3D-printed robotic structure was designed using fused deposition modeling with a polyethylene terephthalate glycol (PETG) composite and integrated with a phased array wheel probe as discussed in [22]. While the 3D-printed design supports structural flexibility, optimizing the trade-off between inspection time and energy-efficient payload handling remains a challenge. This necessitates the development of optimized path planning, alongside further exploration of incorporating NDE sensors for odd-space SHM. A key focus of this research reported in this paper is the role of feedback control, specifically the proportional-integral-derivative (PID) controller, which is widely recognized as the cornerstone of control systems [23]. This study examines PID tuning in the context of a crawler equipped with a phased array probe, performing straight-line path-based motion over a CFRP composite surface under dynamic conditions. Improper tuning can lead to sluggish system response due to increased inertia from high payloads, thereby demanding greater motor power for maneuvering across inclined surfaces. Further, the method utilized for the inspection of the LH2 outer tank was used to check the quality of the C-scan during the inspection of various types of defects.

2. Experimental setup and damage detection methodology

Test goals to create a robust, lightweight tank health monitoring system that can conduct an automatic system examination and operate in an inaccessible area of the tank throughout its lifecycle. The compact robotic crawler can be deployed through the top access port of the tank (250–300 mm), enabling *in-situ* inspection without disassembly or intrusive intervention with intricate conformal geometry and a range of ply thicknesses. In this system, coupling is achieved using water spray, and the probe is integrated into a rolling assembly containing a thin liquid layer that serves as the transmission medium, unlike conventional gel coupling, The ability of the NDI system to detect tank damage as small as 1 mm and allows it to display structural deterioration, including debonding, laminate delamination, and manufacturing-related voids. The overall methodology adopted for the inspection process is illustrated in figure 1. The robot uses an ultrasonic phased array C-scan of the curve surfaces to find defects and ensure safe operation in the time domain based data acquisition. It provides a more thorough depiction by displaying the profile of the material flaw. PAUT methods allow signals to be produced at specific angles and distances. For composites where the anisotropic structure makes signal assessment difficult, these capabilities provide encouraging results.

2.1. Ultrasonic principle

One of the most effective and adaptable ultrasonic testing methods is PAUT, which is particularly useful for intricate geometries. It is crucial to realize that the test findings of ultrasonic testing are influenced by the kind of probes employed, the testing procedure, the ultrasonic wave frequency, the probe position, and the test specimen's material. PAUT uses a phased array probe that has a number of ultrasonic transducers called 'elements,' each of which can independently act as pulser and receiver. Ultrasonic waves can propagate across discontinuities (e.g. inclusions) when they pass through a substance. The wave continues to travel through the material of thickness 't' after hitting a fault, with some of the wave being reflected back to the transducer with n elements (E1, E2, …, and En) as shown in figure 2. After the reflected waves from the edge and defect 'P' strike the transducer, they are transformed back into electrical signals. The A-scan technique offers a straightforward plot of the amplitude of the received signal vs time. Through the movement of the transducer along a line (l), L-scan and C-scan offer a cross-sectional picture of the sample along the width (b) and thickness (t), respectively. Scanning modes like A-scan, L-scan, and C-scan imaging offer high-resolution and high-speed scanning capabilities and are used for comprehensive data display. The property of the Olympus ultrasonic probe is described in table 1. The specimens are ultrasonically inspected using a phased array ultrasonic detector, a linear array probe with 64 unique elements, and a testing frequency of 5 MHz. A frequency of 5 MHz was chosen as an optimal compromise between penetration capability and spatial resolution for the inspected composite structures, with a thickness range of 2–50 mm. The collected data were subsequently analyzed using UT studio software.

2.2. Design of the ultrasonic inspection system

A robotic crawler has been developed for the non-destructive inspection of the LH2 tank under development within the COCOLIH$_2$T project. The inspection system uses a 5 MHz Olympus phased array wheel probe, which is specifically optimized for C-scan ultrasonic evaluation of thick CFRP composites. The 5 MHz frequency of the transducer sets the CFRP's axial resolution and defines the wavelength (λ), which is approximately 0.59 mm. For optimal imaging, the spacing that impacts depth resolution should be less than $\lambda/4$, which is about 0.15 mm. The encoder has a standard resolution of 0.229 mm, but it can achieve a minimal resolution of 0.056 mm when operating in quadrature counting mode. The calculated sampling density is approximately 17.5 samples mm^{-1}, which helps ensure no data is lost. The pulse repetition frequency (PRF) used was 3387 Hz, which is the actual firing rate for the data acquisition unit and is significantly lower than the highest PRF possible with the 5 MHz wheel probe. At this PRF, the maximum allowed crawler speed for data collection is about 190 mm s^{-1}. However, setting the recording speed for NDT equipment has always been difficult because the recording performance typically depends on the acoustic travel time, which is determined by the physics in terms of configuration and resolution; the data throughput, which is dependent on the electronics; and the instrument pulse rate frequency, which is dependent on the physics. Any of the previously listed criteria could be a limiting factor, determining the instrument's maximum recording speed. Each instrument has a maximum rate until it reaches that limit and starts to miss frames. Despite this, the author intentionally selected low, medium, and high speeds that remain within the data acquisition unit's maximum limit. To ensure safe, noise-free collection compatible with the wheel-probe's movement, a PRF was chosen that allows

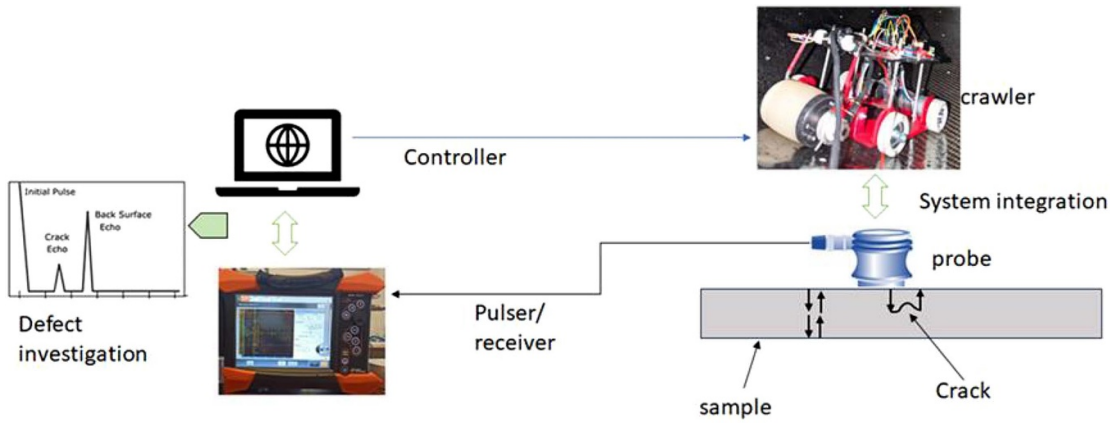

Figure 1. Schematic testing diagram of the sample inspection methodology.

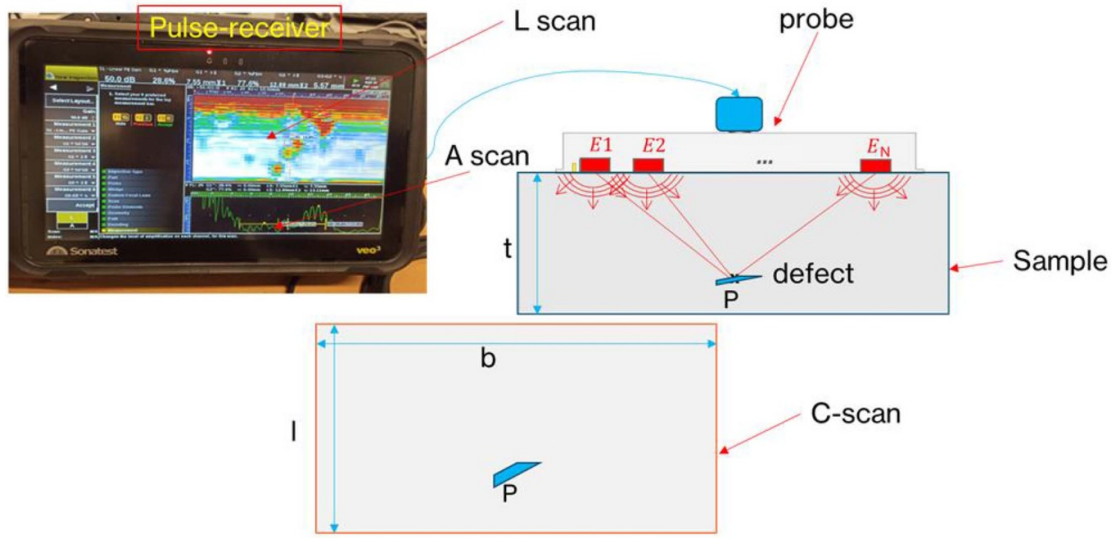

Figure 2. Ultrasonic principle for the damage detection using phased array transducers.

Table 1. The property of the Olympus ultrasonic probe is described in the table 1.

Frequency (MHz)	Delay line height (mm)	Total number of elements	Active elements	Focal law TX	Focal distance (mm)	Elementary pitch (mm)	Active aperture used (mm)
5	25	64	32	16–48	20	0.8	12.8

each echo to return before the next pulse is fired. For active performance, a narrower aperture using 16–32 active elements is selected so the samples achieve the required focal depth; too many elements cause the focus to become blurry and extend too deep. The gain is adjusted so the backwall signal reaches 80% of full-screen height, compensating for CFRP attenuation. Sixteen elements of the transducer are excited over a 100 mm range using a full-wavefield travel mode. The central elements 16–48 are used to match the probe surface's contact curve and to avoid a cracked element near one end of the probe.

2.3. Design of the robotic crawler

The design workflow begins with the conceptual modeling and design of the crawler structure, followed by model preparation for additive manufacturing. The finalized 3D geometry is exported in formats compatible with the PrusaSlicer software, which converts the model into G-code for fabrication. During the slicing process, the model is discretized into layers, with key printing parameters defined as a layer thickness of 0.2 mm for better inter-layer bonding accuracy and strength, printing speed of 60 mm s^{-1}

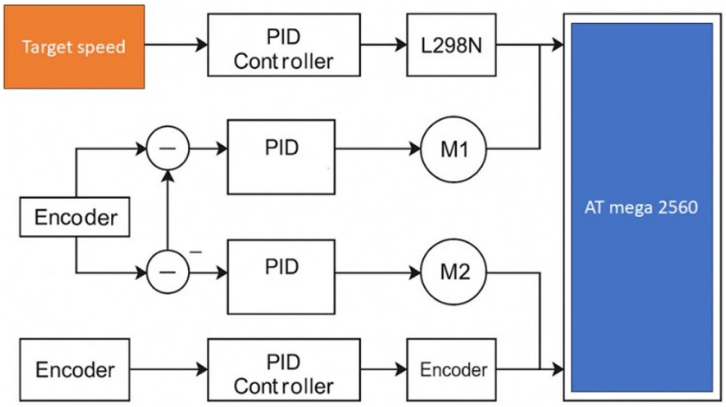

Figure 3. Block diagram of a PID control system for motors.

with travel move of 200 mm s^{-1} in the X–Y directions, and infill density of 50% used for structurally stiff and able to handle the motor torque. The generated G-code is subsequently uploaded to an Original Prusa i3 MK3S+ printer to produce the individual crawler components. After printing, the parts undergo post-processing to remove surface irregularities, improve dimensional precision, and prepare the sub-assemblies for final integration. The assembled crawler structure incorporates two gear motors (M1 and M2) to provide high torque at low speed, each equipped with a 43.8:1 metal gearbox and an integrated quadrature encoder offering a resolution of 700 counts per revolution of the output shaft. Based on this configuration, each encoder count corresponds to approximately 0.224 mm of linear displacement for the crawler during inspection. The encoder data are used to compute the 3D position of the robot and enable PID tuning for precise straight-line motion of the ultrasonic probe. Over 90% of control systems utilize PID due to its effectiveness, their robustness, and straightforward, fixed form, though proper implementation requires significant expertise [23]. A PID controller consists of three components are D (derivative), I (integral), and P (proportional). The processed localization data are translated into standard encoder signals, maintaining full compatibility with conventional ultrasonic acquisition systems [24]. The chosen motors are driven through an L298N motor driver and are rated for an operating voltage range of 1–24 V, with rotation initiating at voltages as low as 1 V. The system targets a payload-to-weight ratio of 3–5:1 with a high 4.7 factor of safety to optimize maneuverability and efficiency. A PID control algorithm regulates the rotational speed of motors (M1 and M2), using encoder feedback to estimate the crawler's position relative to its initial and target locations, as depicted in figure 3. The entire system is powered by a regulated 9–12 V power supply and controlled via an ATmega2560 microcontroller for synchronized motion. The spring based downward force mechanism was introduced to provide proper contact with the inspection surface and navigation along the line.

2.4. Inspected structure with defects

Case I: A curved, 5 mm thick CFRP panel with a radius of 240 mm, a cross-section of 131.5 × 131.5 mm, and a rough, wrinkled surface is used as the first demonstration. This panel was manufactured, damaged by impact, and repaired as described in Shrestha and Groves [25]. In order to detect repaired damage in the structure, as indicated by the color blue in figure 4, the test is carried out remotely utilizing a controller for precise control in path-following for predetermined inspection paths/patterns that might be longitudinal. A 100 mm diameter circumferentially repaired known damage in visibility at the plate's center, as depicted in the panel. However, the damage detection capability was tested for the two extreme points d1 and d2, marked at the circumference, and the direction shown by an arrow.

Case II: The COCOLIH2T (conformal composite liquid hydrogen tank for regional aircraft) consortium, which is proposing a novel double-walled, vacuum-insulated, conformal, thermoplastic composite, low-pressure vessel concept [26]. To provide adequate structural rigidity and pressure resistance, the outside thermoset composite tank has a thickness of 5 mm. A total of 25 plies were utilized to achieve the maximum thickness because the CFRP's cured ply thickness varied between 0.20 and 0.25 mm. Fiber orientations of 0°, 90°, +45°, and −45° were used in a quasi-isotropic lay-up sequence, with subsequent layers rotated by 45°. A number of possible defect types were found to be crucial to the structural integrity of the LH2 tank during manufacturing. Local decreases in compressive strength and stiffness may

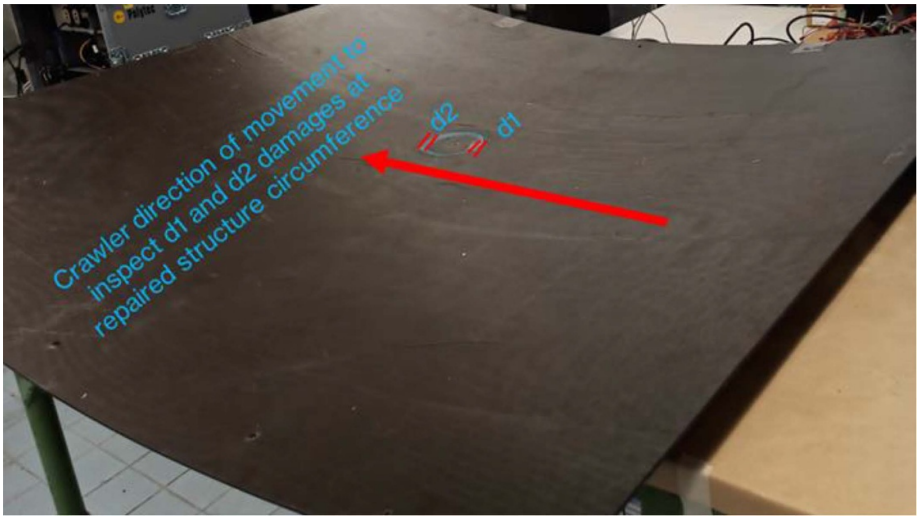

Figure 4. Diagram of the big curve composite structure with repaired damage and inspection line d1 and d2.

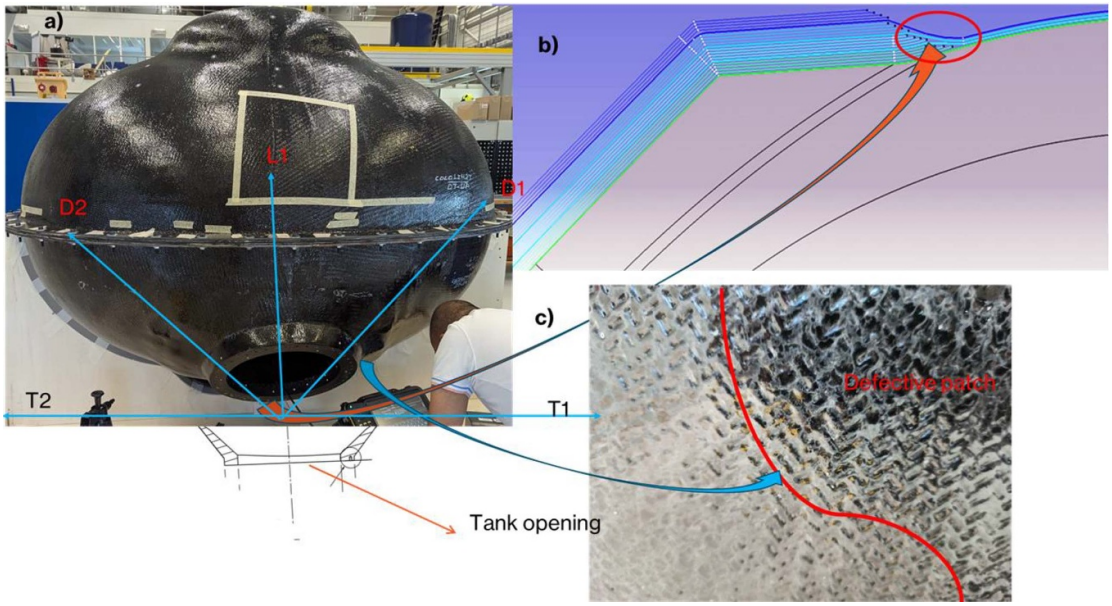

Figure 5. Composite (a) the outer LH2 tank with the tank opening cross-sectional view for the crawler movement for the inspection, (b) ply drop-off, and (c) surface imperfection patches.

result from ply waviness or fiber misalignment in curved areas of the tank, particularly close to tight radii or compound shapes [27]. Ply drop-offs are crucial defect-prone areas where laminate thickness transitions take place, such as at bosses. Abrupt termination of plies can induce interlaminar stress concentrations, leading to delamination or matrix cracking during service [28]. Surface discontinuities, fiber bridging, or incomplete consolidation can also introduce voids and resin accumulation. Components made of composite materials are likely to have different thicknesses in the transition zone and uneven thickness throughout their design. A better probability of detection is needed for particularly close to tight radii or compound shapes than for others, as shown in figure 5(a). Post-manufacturing inspection using an ultrasonic probe is used to identify localized defects such as ply drop-off in the transition zone, as shown in figures 5(b) and (c).

3. Results and discussions

The robotic crawler developed in this study is specifically designed for post-manufacturing quality assurance and scheduled maintenance inspections conducted at ambient temperatures, rather than in-service

monitoring during cryogenic exposure. The cryogenic temperatures (<−253 °C), an extreme operational environment of LH2 tanks, present significant challenges for NDT hardware and acoustic coupling. As the system utilizes water as the ultrasonic couplant, which would freeze in cryogenic states, and PETG components that may undergo embrittlement at extreme temperatures, the current design is optimized for atmospheric conditions and inspection experiment was conducted on a curved CFRP test panel and LH2 outer tank.

3.1. Performance evaluation based on PID response

To validate the crawler's performance, a control and inspection experiment was conducted on a curved CFRP test panel representative of the tank's internal surface geometry. The ability to move with a spring-loaded probe to make sufficient contact on flat and curved surfaces. Navigating the tank's variable curvature was anticipated in the initial model and will be modified to accommodate steep obstacles. Since the behavior of a PID controller on a crawler wheel changes with speed, multi-speed tuning assures that the PID appropriately manages feedback quality, resulting in smooth acceleration, preventing motor drift, and reducing mechanical stress. Single-speed tuning is insufficient for precise and reliable path tracking because curved trajectories enhance speed mismatch errors. Changes in system dynamics, non-linearities, and control resolution constraints are the main causes of this fluctuation. The system's versatility and limitations with the ultrasonic probe were demonstrated by inspecting with different scanning rates (low = 20 RPM = 52 mm s^{-1}, medium = 40 RPM = 104 mm s^{-1}, and high = 60 RPM = 156 mm s^{-1}). Static and rolling friction are more significant at low speeds, whereas inertia becomes more important at high speeds. Furthermore, encoders may have trouble precisely detecting minute movements at very low speeds, producing feedback that is noisy or imprecise. On the other hand, mistakes in velocity estimation could result from missing encoder counts or sampling delays at high speeds. In the first scenario, the real speed finally stabilizes at the intended speed of 60 RPM for M1, as illustrated in figures 6(a) and (b). With a smooth but rather aggressive rising, little overshoot, and steady tracking with a tiny ripple, the system is generally reliable. On the other hand, M2 exhibits a little steady-state error and stabilizes at about 58–59 RPM at 60 RPM, reaching a stable state small overshoot or oscillation. As seen in figures 6(c) and (d), the response at 40 RPM is very well-tuned, achieving a fair balance between proportional gain = Kp, integral gain = Ki, and derivative gain = Kd. These PID settings function best at this setpoint, which determines the strength of the control action. With very little overshoot and steady performance near the target, the response for M2 likewise shows a gradual increase to the setpoint. With minimal operating oscillation and a well-damped response, the M1 response seems well-tuned at 20 RPM, producing a very modest, tolerable steady-state inaccuracy. Nevertheless, M2 responds quickly, with a notable initial overshoot and a continuous oscillation with a minor steady-state inaccuracy.

Out of the three speeds, the 40 RPM response is the most precisely calibrated, offering a quick and precise performance. This implies that for the speed range of 52 mm s^{-1} to 156 mm s^{-1}, the ultrasonic examination requires ideal PID constants (Kp = 0.6, Ki = 0.5, Kd = 0.03). The results of the experiment show that the PID controller successfully lowers steady-state error to 0.5%–1.5% and is resistant to a range of DC motor system disturbances. For DC motor control, manual trial-and-error tuning is safer, more intuitive, and more flexible than the Ziegler–Nichols method, which offers a fast starting point but is often too aggressive, leading to overshoot, continuous buzzing, or outright instability, as seen in figure 7 for 20 RPM. So, trial and error tuning based on Kp, Ki, and Kd values are robust for the multiple speeds, and also maintain the optimize resolution for the investigated PRF vs crawler speed earlier.

3.2. Performance evaluation for damage detection

Based on the samples used and thoroughly explained in section 2.4, the damage detection study is split into two parts. The first section focused on the curved CFRP Panel, while the second one focused on outer LH2 tank. Signal quality of CFRP panel assessed using quantitative metrics such as the signal-to-noise ratio (SNR) and contrast-to-noise ratio (CNR) derived from C-scan amplitude data inspected at three different crawler speeds (52 mm s^{-1}, 104 mm s^{-1}, and 156 mm s^{-1}). Table 2 presents this study while maintaining identical ultrasonic parameters, including gain, focal law, gate settings, and probe configuration. A scan uniformity index based on the coefficient of variation of the background signal stability maintains >99% uniformity, the positional jitter doubles at high speeds, which indicates a reduction in CNR and spatial resolution. One of the best ways to achieve the highest inspection standards is to match the inspection frequency with the thickness of the part.

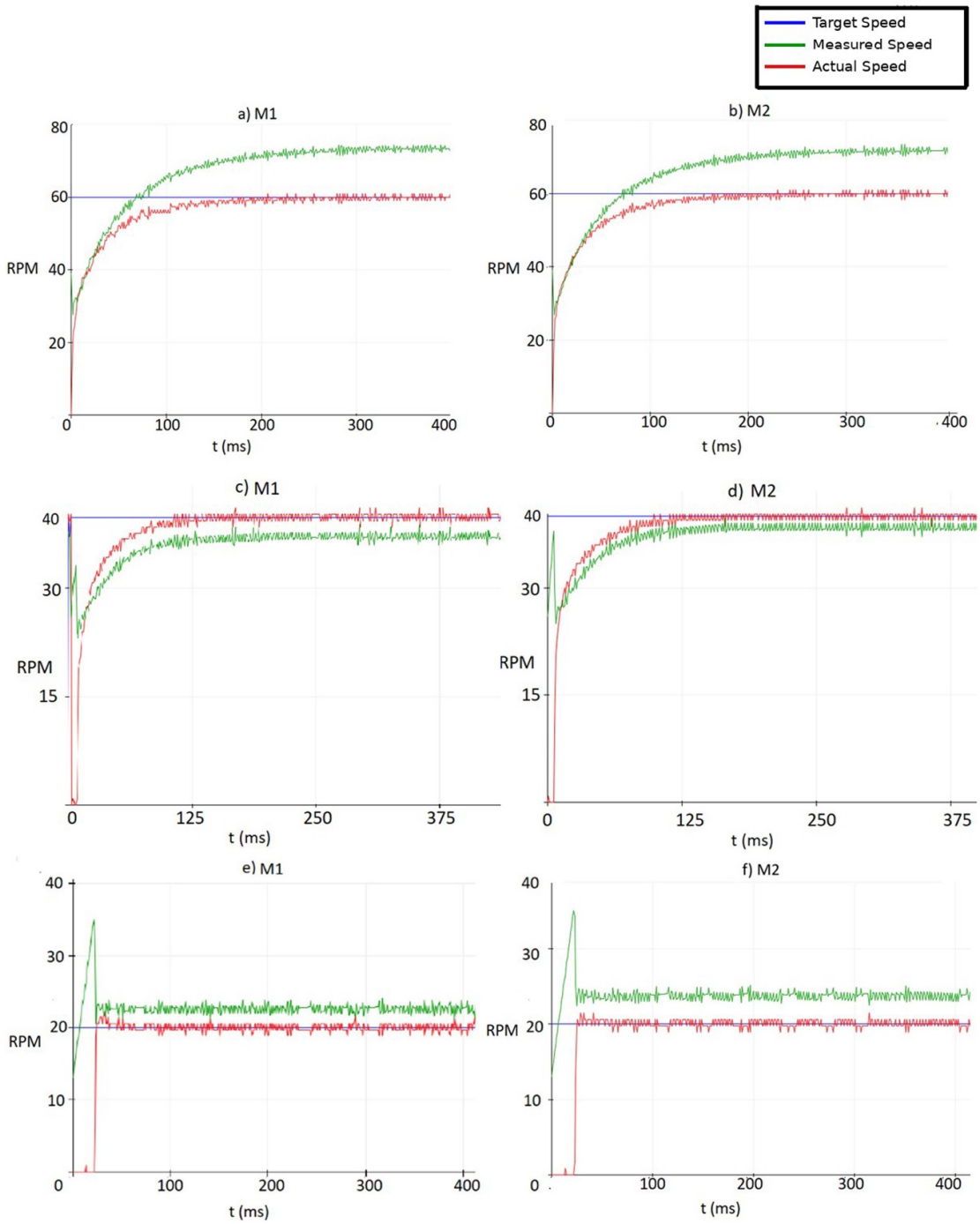

Figure 6. PID tuned response of the both motors at (a) and (b) 60 RPM, (c) and (d) 40 RPM, and (e) and (f) 20 RPM.

Section I: system validation on curved CFRP panel

The test surface intentionally contained a repaired patch and wrinkle features to replicate the realistic conditions of the internal tank wall, as explained earlier and shown in figure 4. The crawler was operated under remote control, using a precision interface to guide its motion along predefined inspection paths. These paths included both longitudinal and transverse trajectories relative to the specimen's geometry, enabling complete surface coverage. Each unidirectional scan was performed with a 12.8 mm probe coverage length. For accurate localization, an encoder system was employed to determine the 3D position of the crawler in real time. A PID control algorithm was implemented to maintain straight-line motion of the 5 MHz phased array ultrasonic wheel probe, with a real-time processing system converting global localization data into standard encoder signals to ensure compatibility with any ultrasonic data acquisition system. Table 3 shows the scan parameters and the structured description for the experimental setup. In figure 8, near the top, there are prominent red and yellow bars (surface reflections). A

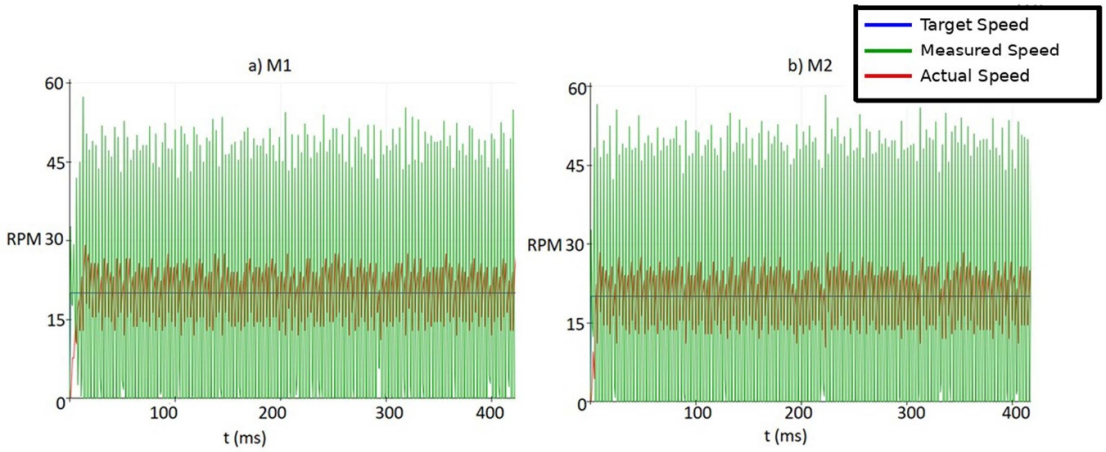

Figure 7. PID tuned response using Ziegler–Nichols method of the motors (a) M1, and (b) M2 at lower speed 20 RPM.

Table 2. SNR and CNR at three different crawler speeds (52 mm s^{-1}, 104 mm s^{-1}, and 156 mm s^{-1}).

Scan speed	Peak amplitude (%)	Background mean (%)	Noise standard deviation	Peak SNR	CNR
52 mm s^{-1}	41.2	37.46	0.12	31.73	24.14
104 mm s^{-1}	40.3	37.08	0.12	27.31	24.41
156 mm s^{-1}	42.65	37.04	0.26	21.57	11.31

Table 3. Parameters and the structured description for experimental setup.

Category	Parameter	Value
Hardware	Pulse voltage	70 V
	Pulse width	150.00 ns (square wave)
Material	Longitudinal velocity	2.970 mm μs^{-1}
Gate settings	G1/G2 threshold	25.0% FSH
	IFT threshold	20.00%
	Acquisition gain	45.0 dB

green/blue transition zone below seems erratic, indicating uneven sound propagation. The lower portion fades to white or blue, suggesting limited backwall return and energy loss. Usually, this pattern shows lateral delamination or debonding throughout the scanned region. Instead of a localized inclusion, the blue zone is a planar defect (delamination) if it is continuous across *X*–*Y*. The C-scan image has vertical bands of somewhat different contrast, but overall, it is a uniform blue. Partial coupling loss or slight thickness fluctuations are frequently indicated by these weak bands, and they support the delamination interpretation. However, the L-scan attenuation region is mostly sound; there may be defect zones near the center where the amplitude drops (25%–30% on scale), indicating a region of fiber distortion or early delamination, most likely due to impact or a resin pocket. A delamination or weak bond area is probably present in the structure close to the mid-thickness of the 5 mm CFRP laminate. The C-scan uniformity drop and L-scan attenuation confirm internal disruption; however, the fault does not cover the whole thickness because some backwall echo is still present.

Section II: robust damage detection in outer LH2 tank

The robotic crawler uses an ultrasonic phased array C-scan of the outer tank's bottom curve surfaces to find defects and ensure safe operation in the time domain based on data acquisition. Damage detection is carried out at the joint of the outer tank as well as inside the tank to check the signal quality, as well as ply drop off and porosity. For this purpose, the crawler was planned with specific transverse, longitudinal, and diagonal directions for the lower half portion due to the symmetrical nature of the opening

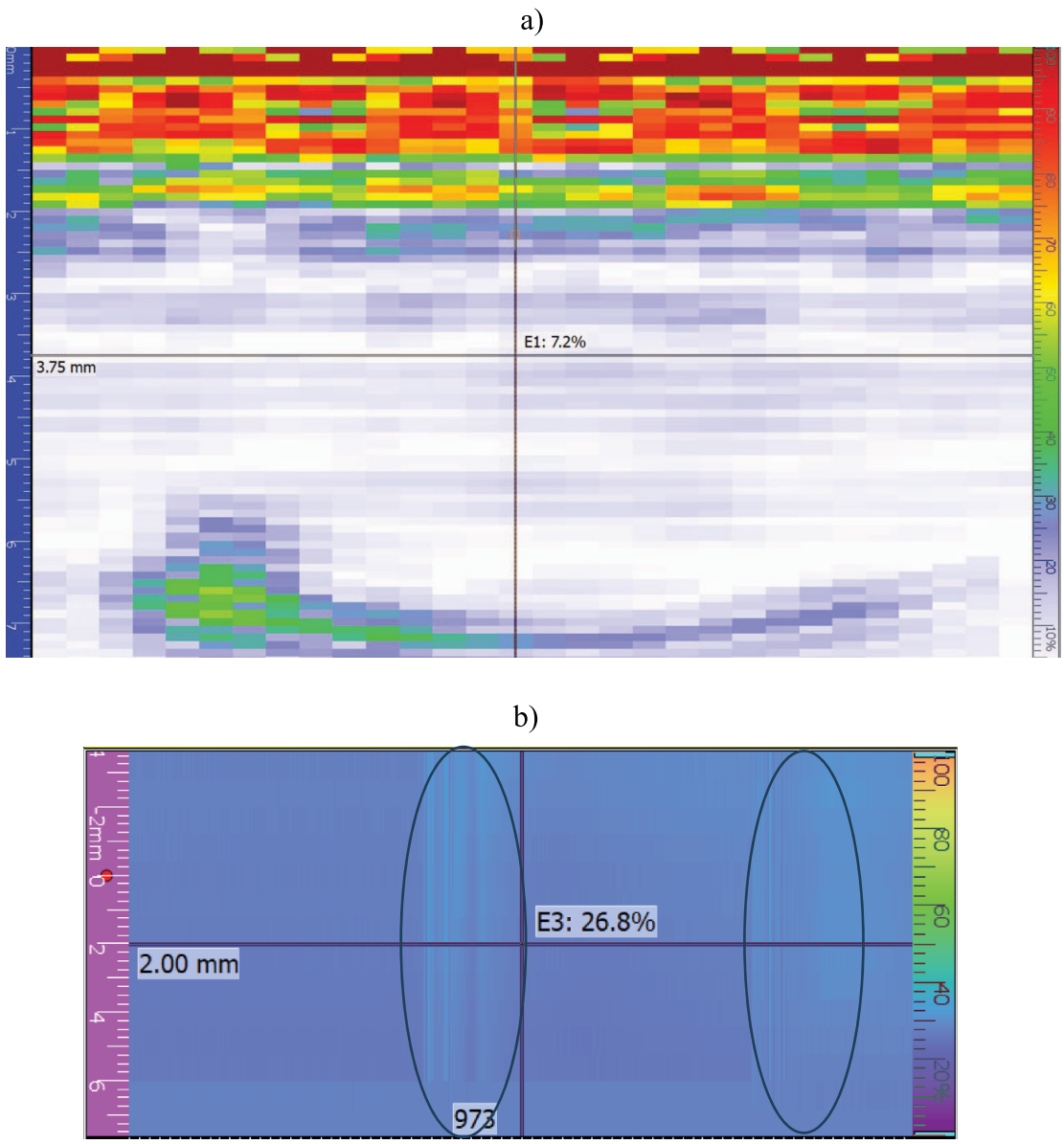

Figure 8. The (a) L-scan and (b) C-scan image for the repaired damage in the structure.

of the outer tank. The inspection carried out at the lower half of the tank at initial stage to study the damage detection capability of the integrated crawler with ultrasonic probe. A detailed description of the experimental process using the ultrasonic testing methods is given in figure 9. The T2T1 direction is considered as the transverse direction. OD1 is the first diagonal, OD2 is the second diagonal, OL1 is the longitudinal direction for the inspection as shown in figure 5. The C-scan, A-scan data using ultrasonic studied by the probe is shown in the figure. The L, B, and C images of the ultrasonic displays are used to evaluate and compare the ultrasonic test findings. In the inspection of OD1 direction, as shown in figure 10, the L-scan and C-scan display a band of greater attenuation at the same depth that extends laterally across multiple frames, resulting in a planar defect or delamination patch instead of a single point inclusion. The crawler was traveling at a very constant speed for the majority of the scan, as seen by the C-scan's smooth, reasonably continuous bands away from the flaw. There are thin, faint vertical streaks at certain frame locations in the C-scan. These may be brought on by encoder jitter, a momentary coupling failure (wheel or membrane lifting slightly), a substantial signal change (material defect), or bigger amplitude changes that align with the fault region. The wheel slide was negligible in this sample because it compresses or stretches the C-scan pattern.

The movement of CFRP laminate is smooth, steady, and appropriately encoded in the OL1 direction as shown in the figure 11; there is no slippage, no pulse loss, no over-triggering or under-triggering,

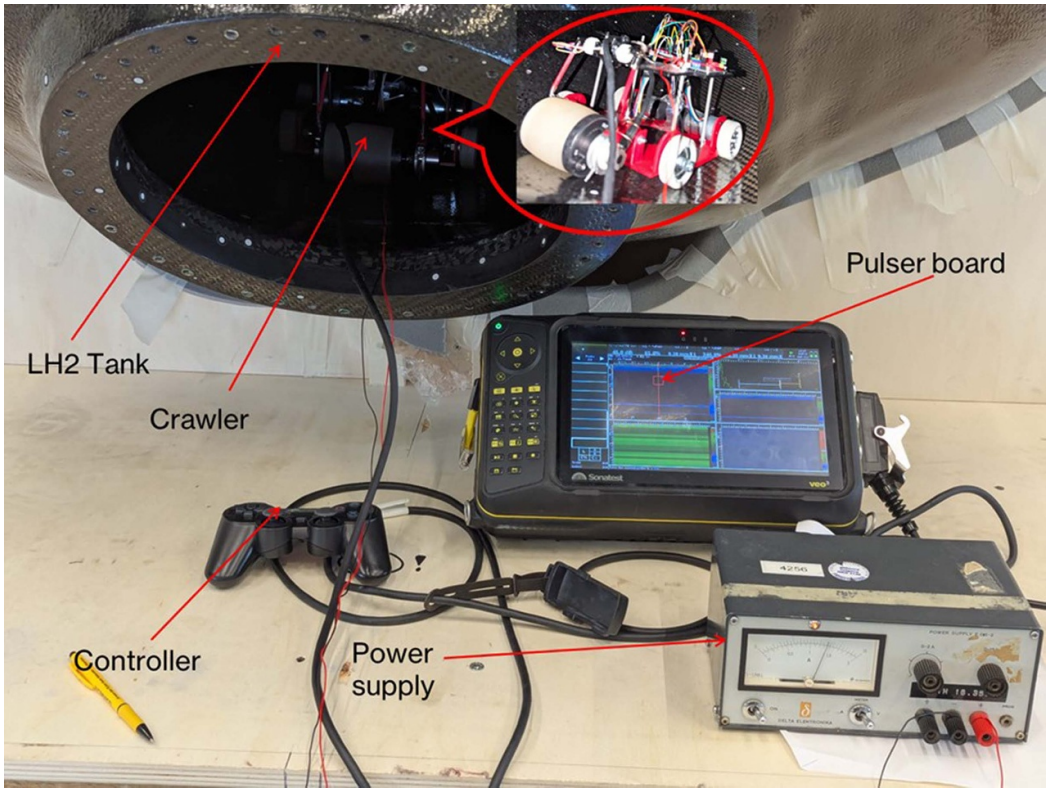

Figure 9. The experimental setup of LH2 tank inspection.

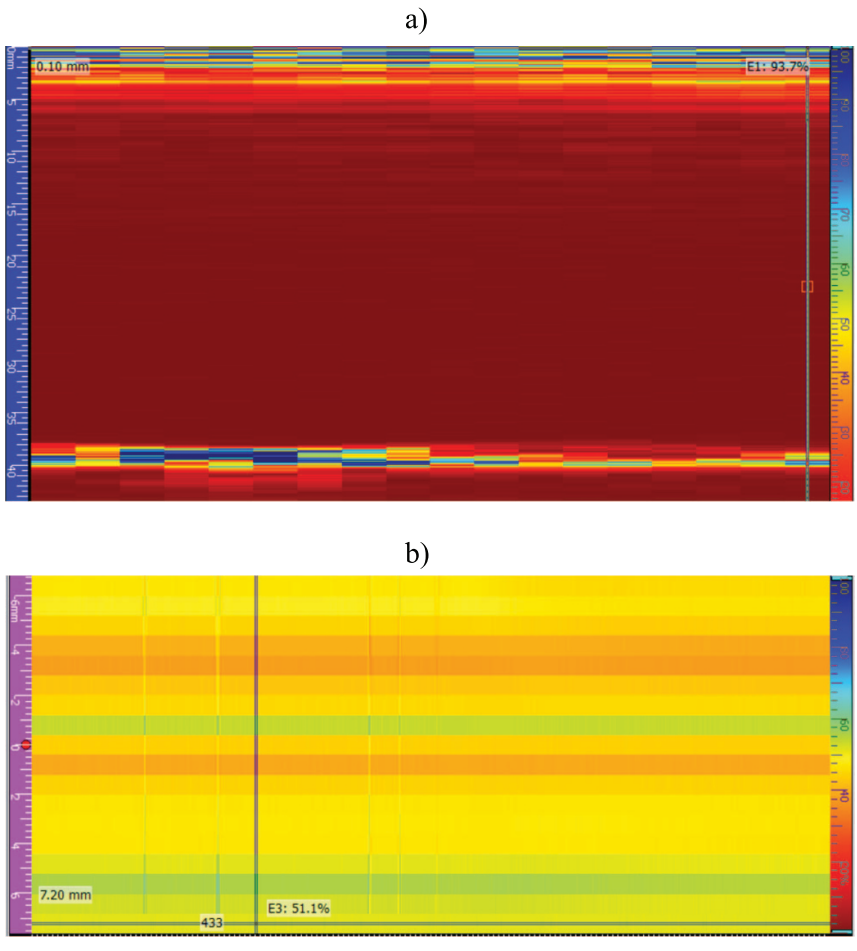

Figure 10. UT (a) L-scan and (b) C-scan image in the OD1 direction.

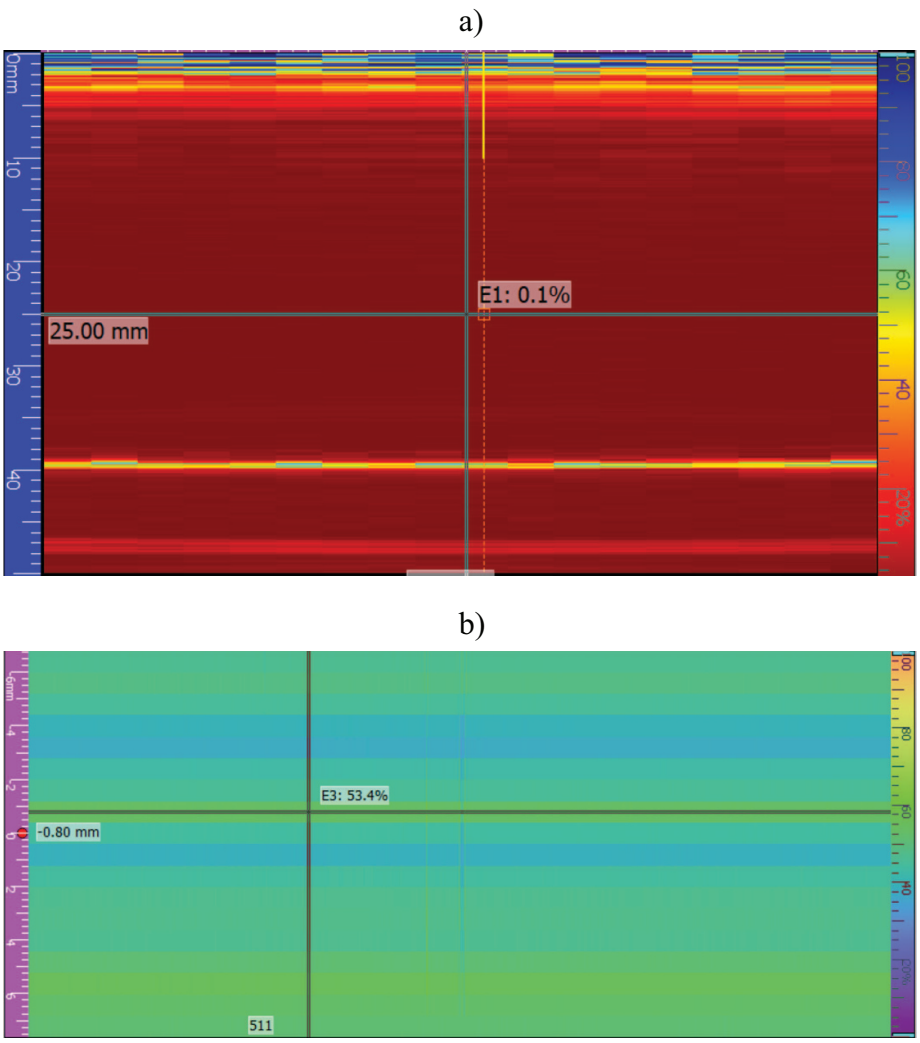

Figure 11. UT (a) L-scan and (b) C-scan image in the OL1 direction.

and no resampling distortion. The material appears structurally sound. Everything is in line with a well-calibrated crawler setup and a healthy laminate. The back-wall amplitude is quite uniform, according to the C-scan. Homogenous background that is mostly green or blue. No bright red areas (overreflection) or dark purple patches (signal loss) which shows no air gap, no resin-starved area, no delamination, no crushed fibers, and no thickness loss. The top region is consistent, and the L-scan reveals stable material with no subsurface flaws, local drop-outs, or intermediate reflector lines.

Sensitivity based on C-scan appears consistent, as shown in figure 12 for the OD2 direction. The signal amplitude is constant because the image is essentially a solid yellow/orange band. The crawler's modest acceleration or deceleration, position jitter from encoder pulses, or a small coupling change during forward motion can cause extremely thin vertical stripes. The structure is acoustically constant and shows no signs of degradation. The vertical lines are scan artifacts rather than structural alterations. With a bright yellow line at the bottom and a strong red/yellow line at the top, L-scan makes the depth-wise behavior more understandable. There is very little noise in the middle zone, which is homogeneous and smooth. Absence of 'hot spots' in the middle. From the L-scan, it can be concluded that there is no laminate split, no crushed core, fiber waviness, or delamination, and the material is homogeneous throughout thickness.

The B-scan in the T2T1 direction obviously reveals a lengthy area of smearing/scattered signals on the *X*-axis as shown in figure 13, which is probably gradual deterioration throughout the scan path rather than a single localized flaw. The B-scan verifies that the damage is extended rather than a spot

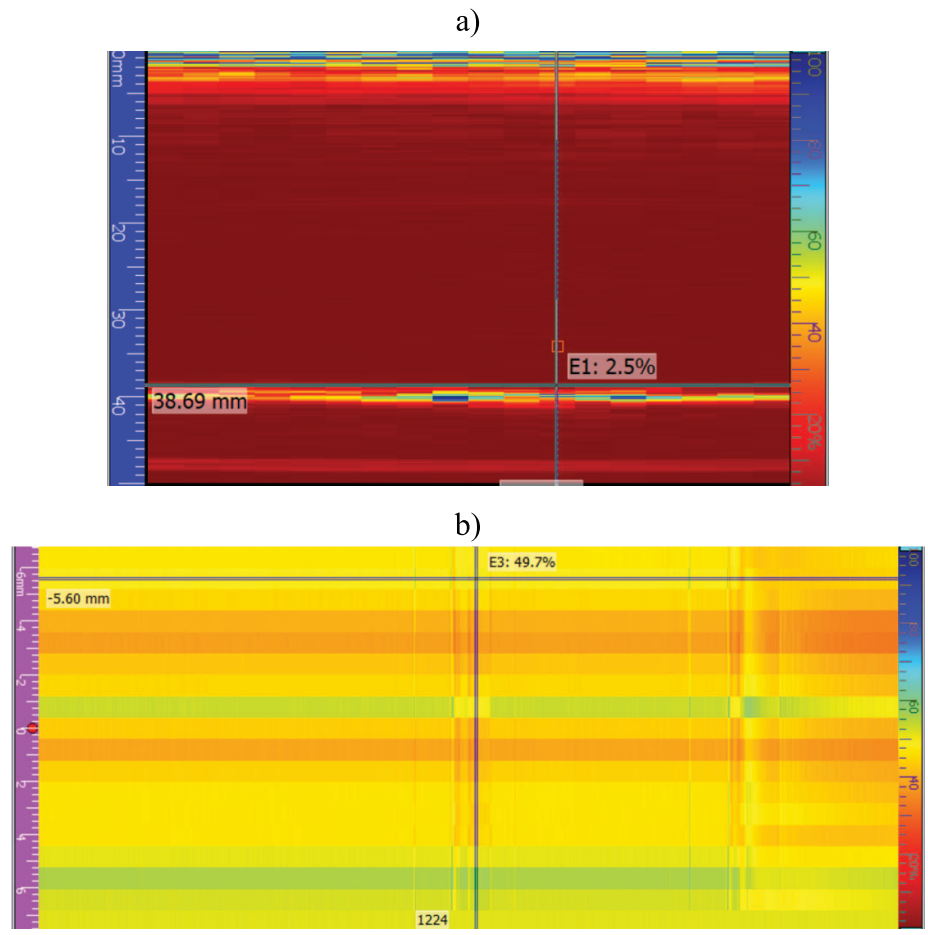

Figure 12. UT (a) L-scan and (b) C-scan image in the OD2 direction.

defect. Since color fluctuations (yellow/green/blue) indicate changes in signal amplitude, the L-scan displays a broad band of variable amplitude probably delamination between CFRP plies or portions that are resin-starved layer-related disturbances. Therefore, the L-scan supports the notion that there are multiple levels of damage rather than a single, deep crack. When B-scan, and L-scan are combined, they show considerable internal damage, and probably multi-ply internal disturbance, which is consistent with a poor curing region. The encoder resolution was sufficient for this scan because the B/L-scan length is constant and not stretched, so there would be no slippage or abrupt leaps.

4. Conclusions

Automated ultrasonic testing is essential for safe, reliable LH2 storage in CFRP tanks, designed to navigate the complex, uneven, thick, and curved surfaces of composite LH2 tanks, providing scalable, efficient, and accurate inspection in order to overcome the drawbacks of traditional NDT techniques for inspecting tanks. This work presents a compact, small access point (250–300 mm), high-payload ratio robot crawler specifically developed for inspecting liquid hydrogen (LH2) storage tanks. The system effectively addressed key inspection challenges such as slippage, surface roughness, and adhesion variation, achieving precise path following and stable localization under dynamic conditions. The crawler integrates precise wheel-encoder-based localization for accurate defect detection, adapted to various speeds, e.g. 52 mm s^{-1}, 104 mm s^{-1}, and 156 mm s^{-1} conditions. PID control tuned via the manual trial and error method and compared with the Ziegler–Nichols method demonstrates its practical smooth application and robustness. Experimental results confirm the effectiveness and superiority of the proposed control scheme at various speeds, particularly 104 mm s^{-1} and below, making this system a promising choice

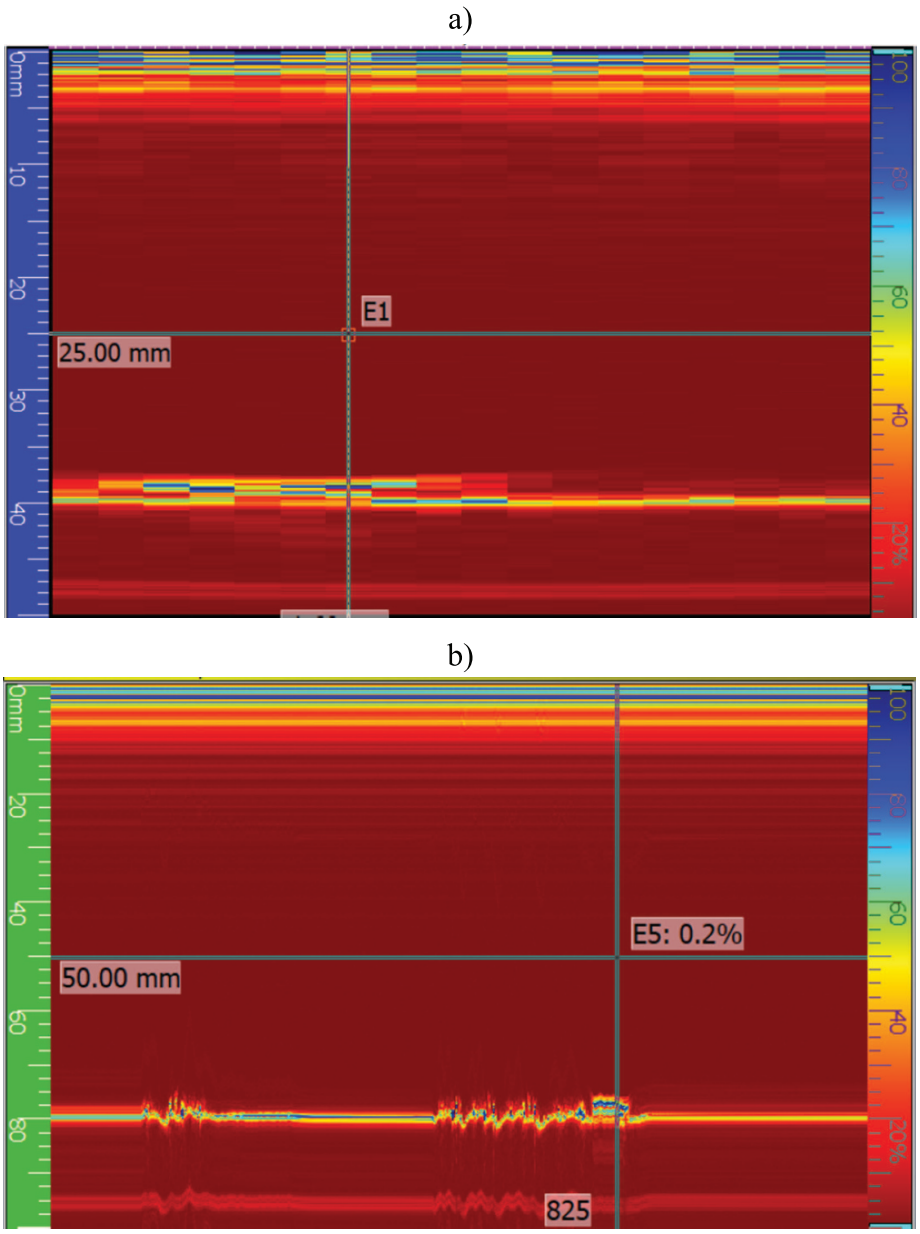

Figure 13. UT (a) L-scan and (b) B-scan image in the T2T1 direction.

for inspection. The ultrasonic inspection of the outer tank focused on assessing the crawler movement on the surface with probe load-carrying capacity and defect detection. The inspection investigates the lower half of the tank with the feasible speed operation on the curved surface. The system shows promising results for the ply drop-off transition zone, where the thickness of the surface changes. Within a CFRP laminate, UT scans reveal a long, shallow internal damage zone along the transverse T2T1 and OD1 axes. The crawler encountered a gradually changing damage region while moving smoothly and without encoder slippage. The investigation successfully detected the outer surface irregularity. The signal characteristics were examined in order to assess the PAUT's capabilities and sensitivity to defects. With a penetration depth of up to 25 mm and minimum detectable fault sizes as small as 0.592/2 mm, according to the Rayleigh criterion [29]. The results demonstrate that PAUT can detect flaws with better characteristics than the traditional ultrasonic approach. In future work, the ultrasonic inspection focused on the inverted movement of the crawler with probe load-carrying capacity and assessing the defect position in the inner tank (57 kg) with a volume of 1100 l.

Acknowledgment

This research was conducted as part of the Horizon EU Clean Hydrogen COCOLIH2T project under Grant Agreement No. 101101404. The project is supported by the Clean Hydrogen Partnership and its members. Views and opinions expressed are however those of the author(s) only and do not necessarily reflect those of the European Union or Clean Hydrogen Joint Undertaking. Neither the European Union nor the granting authority can be held responsible for them. The authors would like to thank the Netherlands Aerospace Centre (NLR) and Novotech for the support in testing.

Data availability statement

All data that support the findings of this study are included within the article (and any supplementary files).

ORCID iDs

Shishir Kumar Singh 0000-0001-6094-8942
Roger M Groves 0000-0001-9169-9256

References

[1] Muradov N Z and Veziroğlu T N 2008 "Green path from fossil-based to hydrogen economy: an overview of carbon-neutral technologies *Int. J. Hydrog. Energy* **33** 6804–39
[2] Yin L, Yang H and Ju Y 2024 Review on the key technologies and future development of insulation structure for liquid hydrogen storage tanks *Int. J. Hydrog. Energy* **57** 1302–15
[3] Manigandan S, Praveenkumar T R, Ryu J I, Verma T N and Pugazhendhi A 2023 Role of hydrogen on aviation sector: a review on hydrogen storage, fuel flexibility, flame stability, and emissions reduction on gas turbines engines *Fuel* **352** 129064
[4] Abohamzeh E, Salehi F, Sheikholeslami M, Abbassi R and Khan F 2021 Review of hydrogen safety during storage, transmission, and applications processes *J. Loss Prev. Process. Ind.* **72** 104569
[5] Salehi F, Talei M, Hawkes E R, Yoo C S, Lucchini T, D'Errico G and Kook S 2015 A comparative study of conditional moment closure modelling for ignition of iso-octane and n-heptane in thermally stratified mixtures *Flow Turbul. Combust.* **95** 1–28
[6] Legault M 2012 Next-generation pressure vessels *High-Perform. Compos.* **20** 40–45 (available at: https://www.compositesworld.com/articles/next-generation-pressure-vessels)
[7] Chi G, Xu S, Yu D, Wang Z, He Z, Wang K and Zhou Q 2024 A brief review of structural health monitoring based on flexible sensing technology for hydrogen storage tank *Int. J. Hydrog. Energy* **80** 980–98
[8] Jodhani J, Handa A, Gautam A and Rana R 2023 Ultrasonic non-destructive evaluation of composites: a review *Mater. Today* **78** 627–32
[9] Shi J, Liu S, Liu F and Xun G 2021 Multi-mode ultrasonic visualization of porosity in composites using a focused transducer with high sensitivity and near-surface resolution *Composites C* **4** 100104
[10] Bai Z, Chen S, Xiao Q, Jia L, Zhao Y and Zeng Z 2017 Compressive sensing of phased array ultrasonic signal in defect detection: simulation study and experimental verification *Struct. Health Monit.* **17** 434–49
[11] Bolotina I, Borikov V, Ivanova V, Mertins K and Uchaikin S 2018 Application of phased antenna arrays for pipeline leak detection *J. Pet. Sci. Eng.* **161** 497–505
[12] Taheri H, Koester L, Bigelow T, Bond L J, Braconnier D, Carcreff E, Dao A, Caulder L and Hassen A A Fast ultrasonic imaging with total focusing method (TFM) for inspection of additively manufactured polymer composite component *Proc. 27th ASNT Research Symp.* (*São Paulo, Brazil, 27–29 August 2018*) pp 212–20
[13] Javadi Y *et al* 2024 Phased array ultrasonic method for robotic preload measurement in offshore wind turbine bolted connections *Sensors* **24** 1421
[14] Tian Y, Chen C, Sagoe-Crentsil K, Zhang J and Duan W 2022 Intelligent robotic systems for structural health monitoring: applications and future trends *Autom. Constr.* **139** 104273
[15] Gucunski N, Basily B, Kim J, Yi J, Duong T, Dinh K, Kee S-H and Maher A 2017 RABIT: implementation, performance validation and integration with other robotic platforms for improved management of bridge decks *Int. J. Intell. Robot. Appl.* **1** 271–86
[16] Xu F, Wang X and Wu H 2012 Inspection method of cable-stayed bridge using magnetic flux leakage detection: principle, sensor design, and signal processing *J. Mech. Sci. Technol.* **26** 661–9
[17] Liu Y-F, Nie X, Fan J-S and Liu X-G 2020 Image-based crack assessment of bridge piers using unmanned aerial vehicles and three-dimensional scene reconstruction *Comput.-Aided Civ. Infrastruct. Eng.* **35** 511–29
[18] Jose J, Elankavi R S, Dinakaran D, Ramya M M and Chetty R M K 2022 The development of ultrasonic C-scan for ferrous wall surface using the climbing robot *2022 7th Int. Conf. on Communication and Electronics Systems (ICCES)* (IEEE) pp 152–8
[19] Ma K S, Lee K-J and Lee J-R 2025 A study on 3D scan-based robot arm control approach for pulse-echo laser ultrasonic testing of curved composite structures *Meas. Sci. Technol.* **36** 045903
[20] Delda R N M, Basuel R B, Hacla R P, Martinez D W C, Cabibihan J-J and Dizon J R C 2021 3D printing polymeric materials for robots with embedded systems *Technologies* **9** 82
[21] Alarifi I M 2023 PETG/carbon fiber composites with different structures produced by 3D printing *Polym. Test.* **120** 107949

[22] Singh S K and Groves R M 2025 Automated crawler-based ultrasonic investigation to monitor the structural integrity of composite liquid hydrogen tanks *Struct. Health Monit. 2025* **3** 2157–64
[23] Singh I 2024 *Control Schemes for DC Motors in Electric Drives* (Pencil)
[24] Li Z 2023 Review of PID control design and tuning methods *J. Phys.: Conf. Ser.* **2649** 012009
[25] Shrestha P and Groves R M 2019 Image analysis for classification of damaged and undamaged areas on composite structures *Proc. SPIE* **10971** 370–7
[26] Noordman B, de Wit B, Creemers R, te Nijenhuis A, Ubels R, Ramaswamy K and Kumar A 2025 Design, analysis and optimization of a vacuum insulated composite conformal LH2 tank *15th EASN Int. Conf.* (*Madrid, Spain*)
[27] COCOLIH2T (COmposite COnformal LIquid H2 Tank) n.d. (available at: www.cocolih2t.eu/)
[28] Ramaswamy K and Wehrle E 2024 Design & optimization of conformal composite liquid hydrogen tank *27th Int. Conf. on Composite Structures (ICCS27)* (University of Bologna)
[29] Krautkrämer J and Krautkrämer H 1990 *Ultrasonic Testing of Materials* (Springer)